World Electric Vehicle Journal

MDPI

Article

Analysis of the Thermal Runaway Mitigation Performances of Dielectric Fluids During Overcharge Abuse Tests of Lithium-Ion Cells with Lithium Titanate Oxide Anodes

Carla Menale [1,*], Antonio Nicolò Mancino [1,*], Francesco Vitiello [1], Vincenzo Sglavo [1], Francesco Vellucci [1], Laura Caiazzo [2] and Roberto Bubbico [3]

[1] ENEA, Centro Ricerche Casaccia, Dip. TERIN, Via Anguillarese 301, 00123 Rome, Italy; francesco.vitiello@enea.it (F.V.); vincenzo.sglavo@enea.it (V.S.); francesco.vellucci@enea.it (F.V.)
[2] ENEA, Centro Ricerche Casaccia, Dip. SSPT, Via Anguillarese 301, 00123 Rome, Italy; laura.caiazzo@enea.it
[3] Department of Chemical, Materials and Environmental Engineering, "Sapienza" University of Rome, Via Eudossiana 18, 00184 Rome, Italy; roberto.bubbico@uniroma1.it
* Correspondence: carla.menale@enea.it (C.M.); nicolo.mancino@enea.it (A.N.M.)

Abstract: Lithium titanate oxide cells are gaining attention in electric vehicle applications due to their ability to support high-current charging and their enhanced thermal stability. However, despite these advantages, safety concerns, particularly thermal runaway, pose significant challenges during abuse conditions such as overcharging. In this study, we investigated the effectiveness of various dielectric fluids in mitigating thermal runaway during overcharge abuse tests of cylindrical LTO cells with a capacity of 10 Ah. The experimental campaign focused on overcharging fully charged cells (starting at 100% State of Charge) at a current of 40A (4C). The tests were conducted under two conditions: the first benchmark test involved a cell exposed to air, while the subsequent tests involved cells submerged in different dielectric fluids. These fluids included two perfluoropolyether fluorinated fluids (PFPEs) with boiling points of 170 °C and 270 °C, respectively, a synthetic ester, and a silicone oil. The results were analyzed to determine the fluids' ability to delay possible thermal runaway and prevent catastrophic failures. The findings demonstrate that some dielectric fluids can delay thermal runaway, with one fluid showing superior performance with respect to the others in preventing fire during thermal runaway. The top-performing fluid was further evaluated in a simulated battery pack environment, confirming its ability to mitigate thermal runaway risks. These results provide important insights for improving the safety of battery systems in electric vehicles.

Keywords: lithium titanate oxide (LTO) anode cells; thermal runaway; dielectric fluids

Citation: Menale, C.; Mancino, A.N.; Vitiello, F.; Sglavo, V.; Vellucci, F.; Caiazzo, L.; Bubbico, R. Analysis of the Thermal Runaway Mitigation Performances of Dielectric Fluids During Overcharge Abuse Tests of Lithium-Ion Cells with Lithium Titanate Oxide Anodes. *World Electr. Veh. J.* **2024**, *15*, 554. https://doi.org/10.3390/wevj15120554

Academic Editor: Hong Zhao

Received: 5 November 2024
Revised: 22 November 2024
Accepted: 25 November 2024
Published: 27 November 2024

1. Introduction

Growing environmental awareness, along with global efforts to reduce greenhouse gasses emissions, has driven a sharp rise in the demand for energy-efficient and sustainable transportation [1]. Among the various powertrain technologies, electric vehicles (EVs) are emerging as one of the most promising solutions. Lithium-ion batteries (LIBs), known for their strong performance and high energy density, have become the dominant energy storage technology for powering EVs [2].

Among lithium-ion batteries, different cathode and anode chemistries are being investigated and utilized based on specific applications. While the most common carbon-based anode materials, such as graphite, offer commendable energy density, the replacement of conventional graphite anodes with lithium titanate ($Li_4Ti_5O_{12}$) has been well documented to provide significant advantages.

Lithium titanate oxide-based (LTO) cells offer a promising alternative to address some of the limitations of traditional lithium-ion chemistries, such as safety concerns (LTO cells are more thermally and chemically stable), cycle life, low-temperature performances, and

fast charging/discharging capabilities. However, despite these advantages, LTO batteries face challenges, including lower energy density and higher material costs, which limit their adoption in the automotive sector. LTO cells are particularly favored when high power density is the primary requirement; consequently, their use is being considered in applications such as commercial vehicles, buses and heavy duty vehicles where factors like charging times and cycle life are critical, while lower energy density represents a minor concern [3–5]. Figure 1 qualitatively summarizes and compares the main characteristics of LTO anode and graphite anode cells.

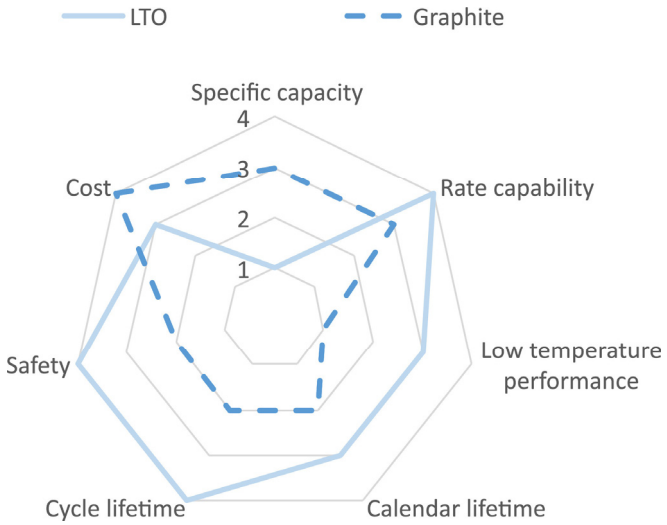

Figure 1. Performance characteristics of LTO and graphite as anode materials in Li-ion battery cells (1: disadvantageous, 4: excellent) [4].

Despite the known benefits of lithium titanate oxide cells, safety concerns remain, particularly in abuse scenarios that can trigger thermal runaway [6,7]. Thermal runaway is a critical failure mode in batteries, particularly in lithium-ion systems [8–13]. It is typically initiated by mechanical, electrical, or thermal abuse conditions that cause an internal short circuit, triggering exothermic chain reactions within the battery. This results in excessive heat generation, leading to an uncontrollable rise in temperature, which may cause fires or explosions. Moreover, even in the absence of external abuse, aging and latent flaws within the battery can act as a triggering factor during its lifecycle [14–17].

The key for preventing thermal runaway lies in ensuring that the battery system operates within safe limits of temperature, voltage, and current. This is typically managed by the battery management system (BMS), which regulates the charging and discharging processes, prevents abnormal current–voltage conditions, and ensures uniform cell charge distribution across a module/pack. Effective energy management is vital for battery safety, as improper energy allocation not only increases consumption but also poses risks of thermal instability and potential hazards. Optimized control strategies improve both energy efficiency and vehicle safety [18]. Robust design, including optimal cell placement within the battery pack, can significantly enhance thermal management. Additionally, various cooling methods, such as air cooling, liquid cooling, phase change materials (PCMs), and hybrid techniques, can be employed to dissipate excess heat during operation [15].

Among various thermal management techniques, direct contact cooling with dielectric fluids stands out as highly effective. Immersion cooling, in particular, achieves superior temperature uniformity within battery packs and individual cells by maintaining direct contact with all the surfaces, thus facilitating more consistent and efficient heat dissipation. Common dielectric fluids used in immersion cooling include hydrofluoroethers, hydrocarbons, esters, silicone oils, and water/glycol mixtures. The effectiveness of these fluids depends on their properties, such as electrical insulation, specific heat capacity, and thermal conductivity. Additionally, many dielectric fluids possess flame-retardant properties, which

are beneficial for preventing thermal runaway and improving battery safety. Specifically, non-flammable fluids or those with high flash points are preferred to mitigate fire risks associated with thermal runaway [19,20].

While prevention strategies focus on avoiding the onset of thermal runaway, mitigation strategies aim to contain and manage its harmful consequences. These strategies operate at different levels [14,21], as follows:

- Material level: Separator materials or flame-retardant additives can help prevent uncontrolled chain reactions.
- Cell level: Internal pressure relief mechanisms, such as gas vents, prevent pressure build-up and reduce the risk of explosions. Devices such as thermal fuses, positive temperature coefficient switches (PTCs), and circuit interrupt devices (CIDs) can cut off the current when critical temperature or pressure thresholds are reached.
- System level: The BMS can isolate specific sections of the battery pack that are at risk. Additional measures include the use of thermal and flame barriers, modular containment, and controlled ventilation systems in large containers to direct gasses away from confined spaces, thereby minimizing fire or explosion risks.

Efforts are underway to develop external mitigation measures, including fire suppression systems, to manage battery fires. A categorization of extinguishing agents used for this purpose includes water, foam, carbon dioxide, dry powder, and halon-based agents. Water-based extinguishing agents are the most economical, largely because of water's high heat capacity and the latent heat of evaporation, which make it particularly effective in fighting battery fires [15].

However, water's electric conductivity represents a drawback, as it can cause external battery short circuits, potentially leading to the propagation of thermal runaway. Foam-based extinguishers work by creating a barrier between the high-temperature surface and flammable vapors or gasses. For maximum effectiveness, the foam must fully cover the battery surface, as any air passing through the foam can sustain the fire. Carbon dioxide (CO_2) extinguishers, though safe for use around electrical components, have limited cooling capacity, reducing their overall effectiveness. Additionally, CO_2 can pose respiratory risks in enclosed spaces. Dry powder extinguishers act by disrupting the chemical reactions that sustain the fire but do not provide cooling, which increases the risk of re-ignition. Similarly, halon-based agents chemically inhibit combustion without leaving any residue, but they also lack cooling properties. Furthermore, halons have adverse environmental effects, contributing to global warming and ozone depletion [15,22,23].

Although many studies explore dielectric fluids for immersion cooling, the use of these liquids as a mechanism or strategy to mitigate thermal runaway reactions is rarely addressed in the literature. This study aims to evaluate the effectiveness of immersion cooling systems—traditionally employed for thermal management in battery packs—in suppressing or mitigating thermal runaway once the process has been initiated. Specifically, the research focuses on assessing the performance of dielectric fluids in mitigating thermal runaway in 10 Ah cylindrical lithium titanate oxide cells caused by overcharging. The study compares four different fluids: two perfluoropolyether fluorinated fluids (PFPEs) with varying boiling points, a silicone oil, and a synthetic ester.

2. Experimental Set-Up

The experiments were conducted at the ENEA Casaccia Research Center, specifically within the FARO facility (see Figure 2). Covering approximately 900 square meters, the FARO facility includes specialized infrastructures, such as a control room and dedicated storage areas, to manage high-risk experimental trials safely. The facility is designed to handle scenarios involving fires, explosions, and other hazardous events. For this study, it was utilized for the abuse testing of batteries.

The abuse tests described in this study were conducted using a portable cycler, IT6005C-80-120 (5 kW, voltage range: 0–80 V, maximum charge/discharge current: 120 A). In order to ensure consistent initial conditions, each cell underwent standard charge/discharge

cycles prior to the test, using a Digatron cycler, MCT 250-06-12 RE (voltage range: 0–6 V, charge current range: 0.3–250 A; discharge current range: 0.3–250 A, charge/discharge peak current: 300 A for 10 s per minute).

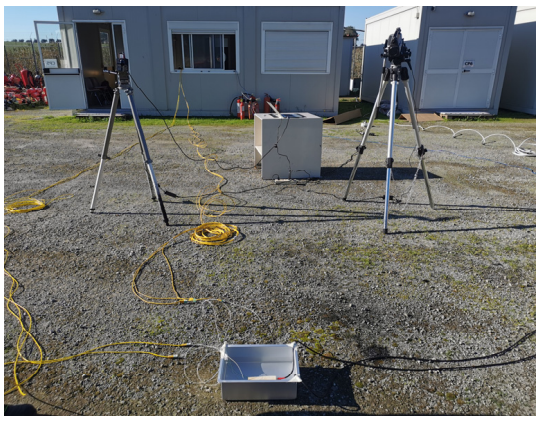

Figure 2. FARO plant and test set-up.

The monitoring of the cells under testing was conducted using the following equipment:

- High-Speed Cameras: These cameras were used to capture rapid dynamic phenomena during overcharge abuse tests. Their ability to record events at high frame rates allowed precise observation and documentation of critical events such as cell swelling, rupture of the cell bottom, venting, explosions, and flame generation. The Redlake MotionPro Y3S1-M Fast Camera (recording frame rate: 3000 fps; resolution: 1280 × 1024) and the DS-CAM-320c Fast Camera (recording frame rate: 328 fps; VGA resolution: 640 × 480) were used for this purpose.
- Thermal Camera: A thermal infrared camera was employed to monitor surface temperature changes in the cells during open-air tests. It provided non-contact temperature measurements, enabling the detection of the maximum surface temperature even in the case of thermocouples' detachment. The model used was the Flir S60 Thermal Infrared Camera, with maximum temperature measurement of 1500 °C, thermal sensitivity < 0.1 °C, and accuracy ±2 °C or ±2%.
- Type K Thermocouples: Positioned on the surface of each tested cell, type K thermocouples provided precise temperature measurements at specific points on the cell surface, offering high-accuracy localized readings (accuracy of ±0.1 °C).
- National Instruments "CompactDAQ" Chassis: This hardware, equipped with a module for thermocouple data acquisition (24-bit ADC, 16 channels), was used to collect and digitize the data from thermocouples in real time. Its high resolution ensured the accuracy and fidelity of the temperature measurements, which are critical for evaluating the cells' response to abuse conditions.
- Data Acquisition System: This system was designed using LabVIEW. This system was designed to efficiently collect and record data from the monitoring instruments. It facilitated real-time data acquisition and provided a user-friendly platform for organizing the data collection, ensuring accurate documentation of the cells' responses during overcharge abuse testing.

In all tests, overcharging current and cell voltage were directly measured by the portable cycler.

2.1. Test Configurations

In the experiments, the thermal runaway behavior of the cell was investigated to compare the occurrence and severity of the phenomenon under ambient air conditions and with the cell immersed in a specific dielectric fluid. For both the above conditions, two different test configurations were considered (Figure 3):

a Overcharging of a single LTO cell.
b Overcharging of an LTO cell within a battery pack scenario.

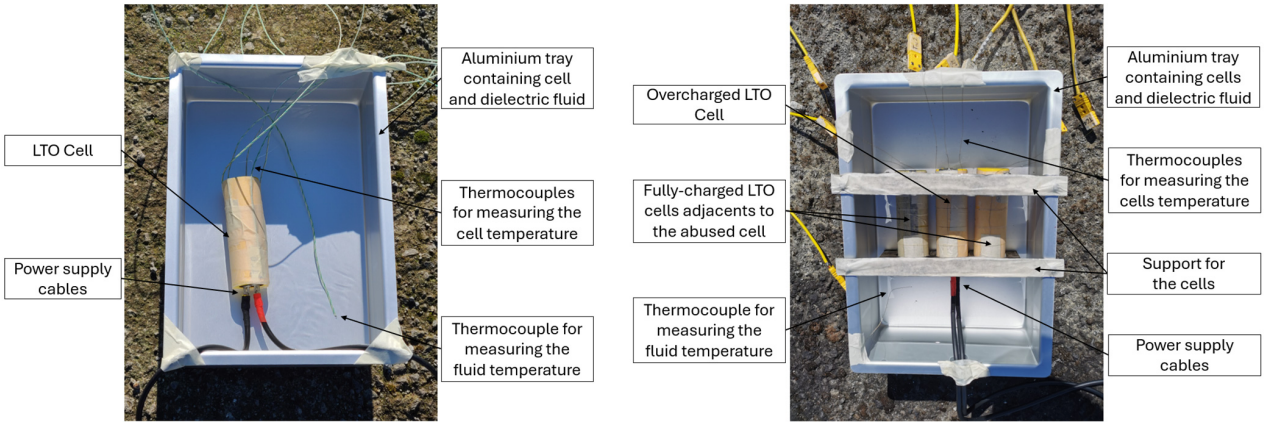

Figure 3. Test configuration: (**a**) overcharging of a single LTO cell; (**b**) overcharging of an LTO cell within a battery pack scenario.

The primary objective of the first test configuration (Figure 3a) was to assess the effectiveness of dielectric fluids in mitigating thermal runaway events during the overcharge abuse of a single cell. In this configuration, the cell was equipped with five thermocouples and shielded using adhesive paper to allow accurate surface temperature visualization via the thermal imaging camera. The cell was located in an aluminum tray and connected to the bidirectional power supply. In the initial benchmark test, under open-air conditions, a sixth thermocouple (TL) was positioned near the test site to measure the ambient temperature. For the subsequent four tests, the tray containing the cell was filled with different dielectric fluids and the fluid temperature was measured by placing this thermocouple inside the liquid (not directly in contact with the cell surface).

Once the most effective fluid for the thermal runaway mitigation of a single cell had been established, the second test configuration was used to perform in-depth tests evaluating the influence of an LTO cell under thermal runaway on adjacent cells in a battery pack scenario. To simulate this condition, a support structure was created to hold three LTO cells at a fixed distance within the container, with a typical spacing of 0.5 cm between the cells [24]. Once again, in this second test configuration, shown in Figure 3b, both the open-air condition and the selected dielectric fluid bath were performed and compared.

Figure 4 shows the thermocouple locations for the two test configurations.

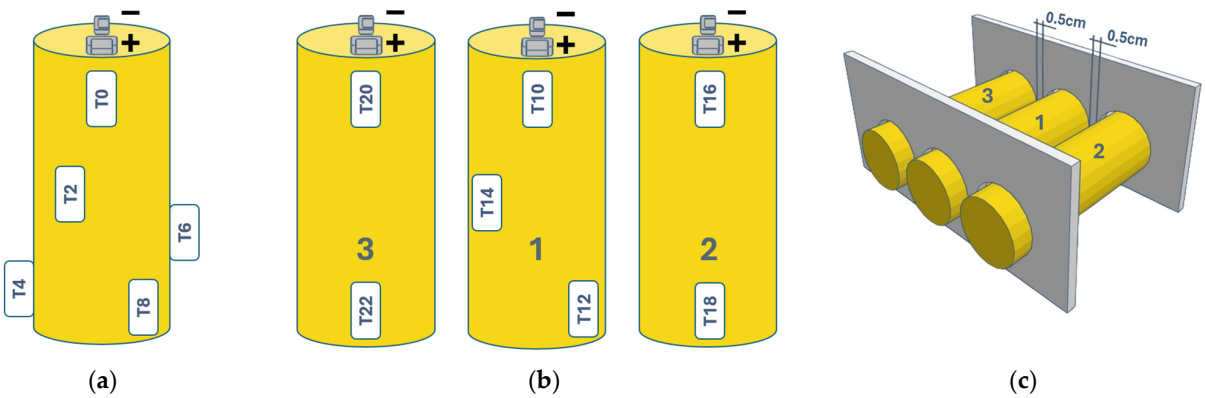

Figure 4. Thermocouple location on the cell surface: (**a**) thermocouple location for the first test configuration; (**b**) thermocouple location for the second test configuration; (**c**) layout of the second test configuration.

2.2. Materials

The experimental tests were performed by overcharging fully charged cells (initial State of Charge = 100%) with a current of 40A (4C). Table 1 describes the main characteristics of the cells.

Table 1. Properties of LTO cells.

Nominal Capacity	Nominal Voltage	Max. Charge Voltage	Standard Charge	Charge Temp. Range	Dimensions (D × H)	Weight
10 Ah	2.4 V	2.8 V	5 A	−20 °C to +50 °C	40 mm × 120 mm	280 ± 10 g

Four different dielectric fluids were tested to evaluate their effectiveness in mitigating or containing potential fires or explosions:

- Two high-performance inert (non-flammable) fluorinated fluids: These fluids offer excellent chemical stability and can operate at both very low and high temperatures in harsh conditions. Specifically, two fluids with different boiling points were selected (Table 2): PFPE170, characterized by low kinematic viscosity but a lower boiling point, and PFPE270, which exhibits a higher boiling point and is characterized by higher kinematic viscosity.
- One synthetic ester, a non-volatile, single-phase fluid: This is a biodegradable, non-toxic liquid with fire safety properties (high flash and fire points) and robustness. The selected fluid was previously tested for the thermal management of lithium-ion batteries.
- One silicone oil: An eco-friendly fluid with a high flash point and excellent thermal stability.

Table 2. Properties of dielectric fluids.

Fluid	Cp @ 25 °C (J/kg K)	k @ 25 °C (W/m K)	ρ @ 25 °C (kg/m^3)	μ @ 25 °C (mm^2/s)	T_b (°C)	Flash Point (°C)	Fire Point (°C)
PFPE [1] 170	961	0.065	1770	1.80	170	-	-
PFPE [1] 270	961	0.065	1850	14	270	-	-
Synthetic Ester	1902 [2]	0.147 [2]	968 [2]	75 [2]	n.a.	>250	>300
Silicone Oil	1498	0.14	1065	125	>65	333	-

[1] Perfluoropolyether; [2] @20 °C.

The selected fluids were chosen based on a previous study [25] which evaluated commercially available fluids according to key properties essential for effectively mitigating or containing the effects of potential fires or explosions. The main properties included the following:

- Thermal Efficiency: The fluid should effectively remove heat under natural convection; this property should be evaluated by considering the fluid's specific heat capacity, thermal conductivity, and viscosity.
- Boiling Point: It should be high enough to prevent vapor formation, which could increase fluid volume and cause mechanical damage.
- Flash Point/Fire Point: This should be as high as possible to prevent possible combustion of the fluid.

The main properties of the adopted fluids are shown in Table 2.

3. Results and Discussion

3.1. Single-Cell Tests

Recording each test using the fast cameras allowed for the analysis of the different behaviors of the cells under the tested conditions. Figures 5–9 show the most relevant frames, highlighting the different phases of thermal runaway and their consequences.

In these sets of figures, the first frame consistently depicts the initial conditions of the cell at the beginning of the test. The second frame shows the rupture of the cell bottom due to the internal accumulation of venting gasses. The third frame provides a visualization of the venting phenomenon. The subsequent frames capture the final outcomes, including, where applicable, the moment of the explosion. In the tests involving synthetic ester and silicone oil, three distinct frames are shown, referring to explosion, ignition, and post-explosion flames.

A detailed description of each test follows.

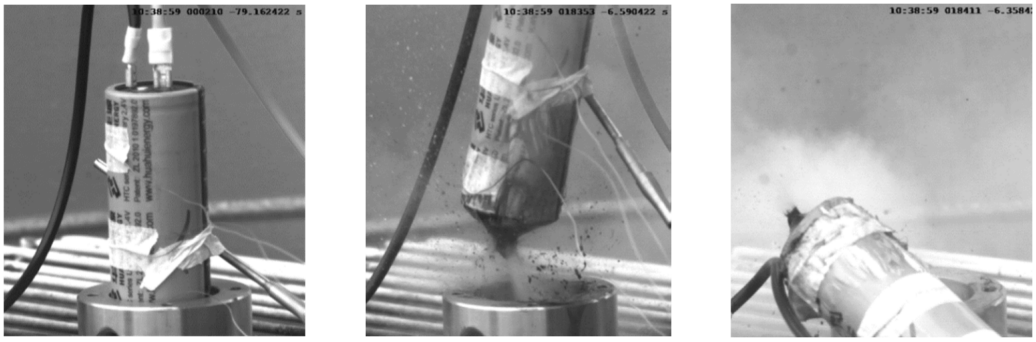

(**a**) (**b**) (**c**)

Figure 5. Open-air test sequence: (**a**) before venting, (**b**) bottom failure due to venting. (**c**) venting.

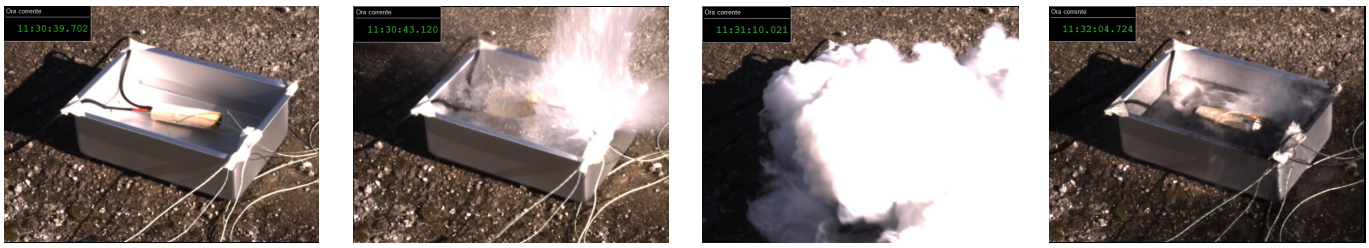

(**a**) (**b**) (**c**) (**d**)

Figure 6. Cell immersed in PFPE-170 sequence: (**a**) before venting, (**b**) bottom failure due to venting, (**c**) intensive venting, (**d**) after intense venting.

(**a**) (**b**) (**c**) (**d**)

Figure 7. Cell immersed in PFPE-270 sequence: (**a**) before venting, (**b**) bottom failure due to venting, (**c**) intensive venting, (**d**) flames after intense venting.

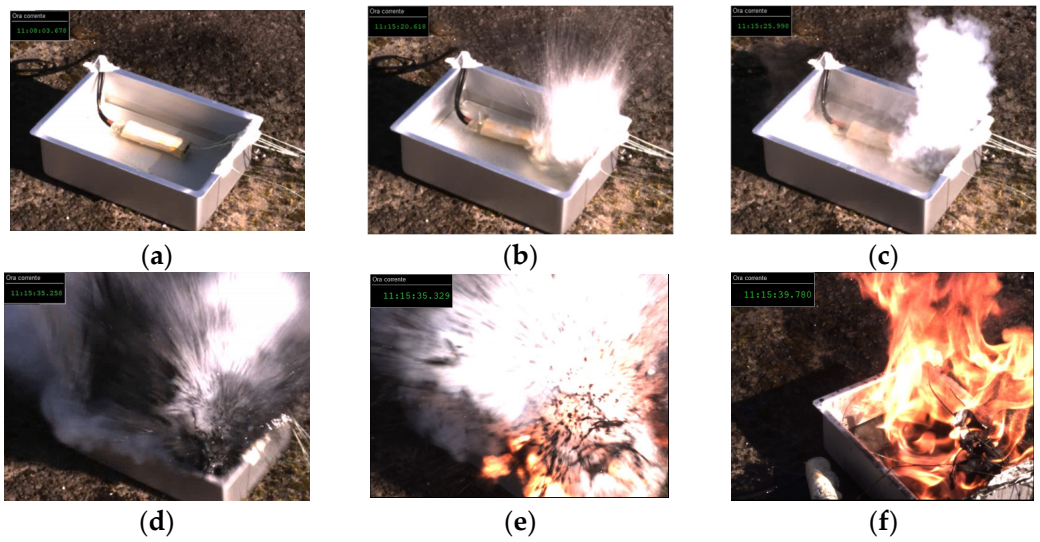

Figure 8. Cell immersed in synthetic ester sequence: (**a**) before venting, (**b**) bottom failure due to venting, (**c**) intensive venting, (**d**) second explosion, (**e**) fire generation during the explosion, (**f**) flames after intense venting.

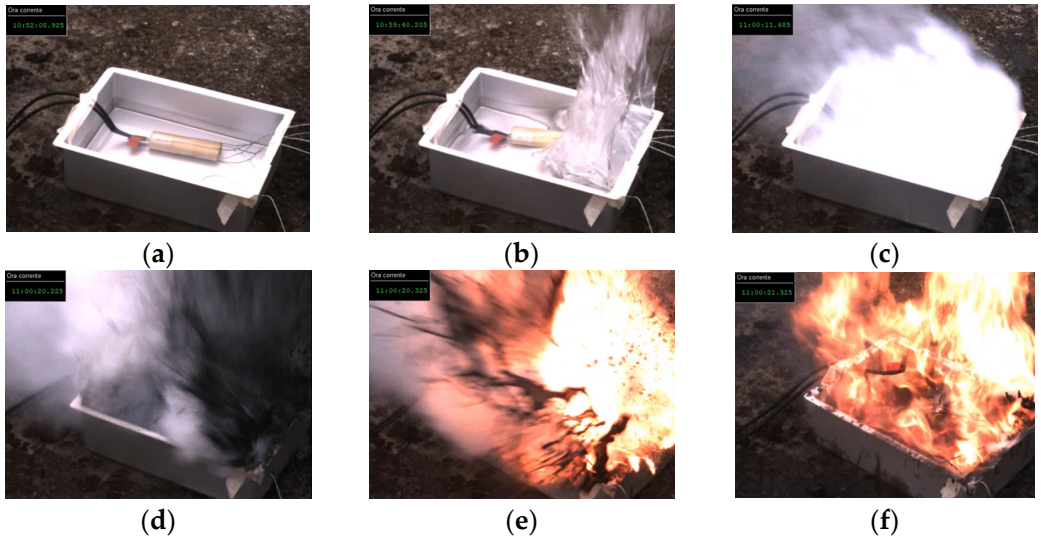

Figure 9. Cell immersed in silicone oil sequence: (**a**) before venting, (**b**) loss of the bottom due to venting, (**c**) intensive venting, (**d**) second explosion, (**e**) fire generation during the explosion, (**f**) flames after intense venting.

The overcharge abuse test of the LTO cell in open-air conditions was characterized by an initial swelling of the cell and a subsequent rupture of the cell bottom (opposite side to the electrodes). Following the initial venting phase, the cell exploded; unfortunately, the explosion was not captured on video, as the cell had moved out of the camera angle due to the initial venting phase. The use of PFPE dielectric fluids reduced the magnitude of the explosion effects (Figures 6 and 7); however, the generation of a significant volume of gas was observed, primarily due to dielectric fluid evaporation. Furthermore, during the test with PFPE 270, a small flame was detected on the battery (Figure 7d), and only on the battery, while no flames were detected with the use of PFPE 170. On the other hand, the use of synthetic ester and silicone oil proved to be detrimental from a safety perspective: in both cases, after the initial overcharge, cell bottom loss, and abundant venting gas release, a strong explosion and severe flame generation from both the battery and the liquids were recorded (Figures 8 and 9).

Following the qualitative description of the cell behavior, the characteristic times of the experiments are now defined to accurately quantify the dynamics of the observed phenomenon. Under overcharge conditions, the cell voltage typically rises to a peak before decreasing due to internal damage. During this phase, the cell begins to produce reaction gasses, leading to swelling of the cell case. Once the internal pressure exceeds a critical threshold, the cell's bottom, specifically designed to be the weakest part of the case, ruptures. This is followed by a phase of gas venting from the bottom of the cell, ultimately culminating in a catastrophic cell explosion. Based on this typical sequence, the following time intervals were defined:

- Time to maximum voltage t_{Vmax}: The time interval from the start of the test to the point when the cell reaches its maximum voltage.
- Time to thermal runaway on-set t_{TR}: The time interval from the test start to the onset of thermal runaway defined following the definitions set by the UNECE Global Technical Regulation No. 20—Electric Vehicle Safety (EVS) (ECE/TRANS/180/Add.20) [26]. In particular, following the recommendation by Bruchhausen et al. [27], who compared different criteria established by UNECE EVS, ISO 6469-1/Amd 1 (ISO 6469-1:2019/Amd 1:2022, 2022), and by the Chinese national standard GB 38031 (GB 38031:2020,2020), the two most pertinent criteria are as follows:
  - $T_{ref} > T_{maxop}$, where T_{ref} is the temperature near the electrodes and T_{maxop} is the cell's maximum operational temperature (according to the datasheet of this cell, $T_{maxop} = 50\ ^{\circ}C$ in charge conditions);
  - $\frac{dT_{ref}}{dt} > 1$ K/s for a minimum duration of $\Delta t = 3$ s, specifically for cells with an energy density below 130 Wh/kg.
- Time to rupture t_r: The time interval from the start of the test to the rupture of the cell's case bottom (identified from the fast camera recordings).
- Time to fire t_{ex}: The time interval from the start of the test to the final explosion or flame generation—if applicable (identified from the fast camera recordings).
- Total test time t_{Tmax}: The time interval from the start of the test until the cell reaches its maximum surface temperature.

Table 3 provides a summary of the time intervals for the various test phases.

Table 3. Timeline of the thermal runaway phases.

Test	t_{Vmax} [s]	t_r [s]	t_{TR} [s]	t_{ex} [s]	t_{Tmax} [s]
Open Air	273	374	374	n.a. [1]	420
PFPE 170	380	447	466	-	504
PFPE 270	334	412	424	444	456
Synthetic Ester	350	442	449	457	476
Silicone Oil	376	460	493	500	515

[1] The final explosion occurred outside the high-speed camera's field.

In terms of timing, the use of a dielectric fluid delayed the thermal runaway phenomenon. In fact, the maximum cell voltage was reached later when containment fluids were used, compared to the open-air test. The delay in reaching the maximum voltage, relative to the open-air test, was calculated for each fluid. PFPE 170 exhibited the most significant delay of 107 s, followed by silicone oil (103 s), synthetic ester (77 s), and PFPE 270 (61 s). The thermal runaway onset of the cell was delayed by varying time intervals depending on the fluid adopted, with silicon oil providing the largest delay, followed by PFPE 170. These delays were supported by the enhanced thermal exchange properties of the fluids compared to air.

The graphs in Figures 10–13 illustrate the trends in supply voltage and cell surface temperatures across the different tests, focusing on the temperature rise caused by the thermal runaway. These figures also depict the dielectric liquid temperature. For the sake of clarity, temperature readings from the thermocouples are reported starting from 400 s, as previous measures are nearly uniform. The curves continue until the maximum temperature recorded during each test is reached. When explosions caused the detachment of some thermocouples from the cell surface before reaching the peak temperature, the corresponding temperature curves are displayed only up to the detachment point.

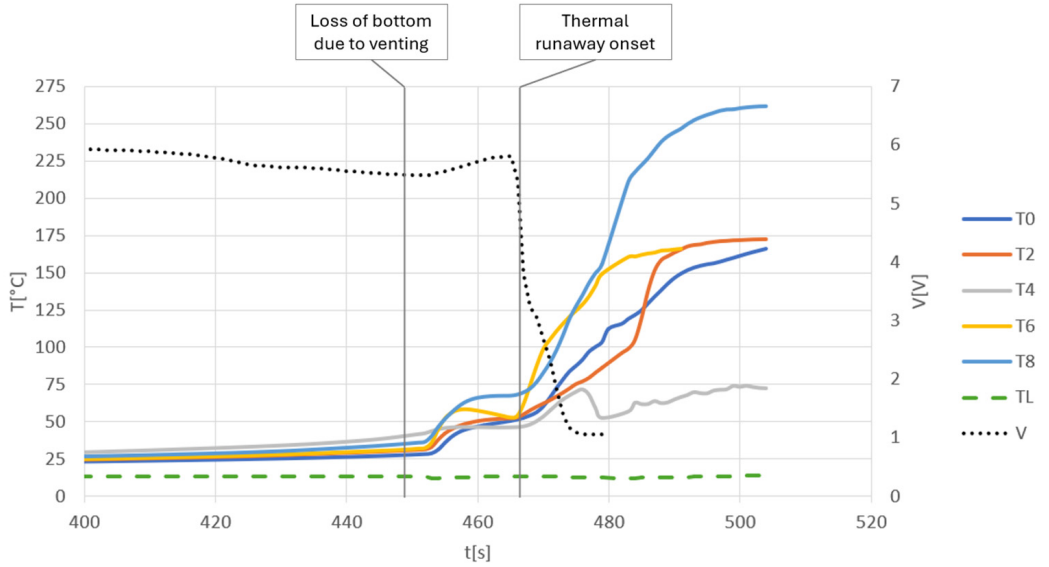

Figure 10. Temperature values of thermocouple T0-T8 on the surface of the cell; TL, temperature of the liquid and supply voltage for the test with PFPE170.

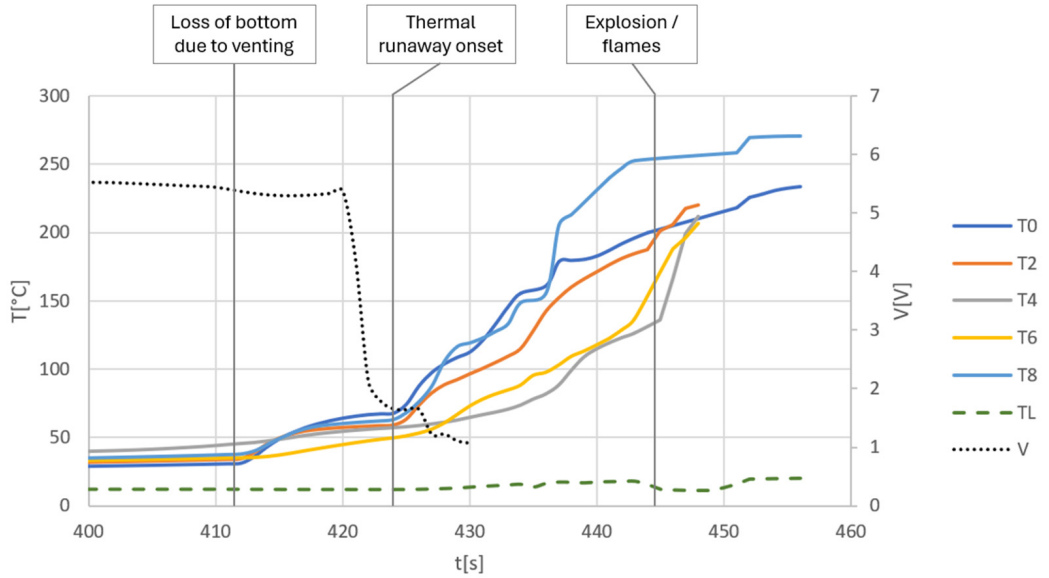

Figure 11. Temperature values of thermocouple T0-T8 on the surface of the cell; TL, temperature of the liquid and supply voltage for the test with PFPE270.

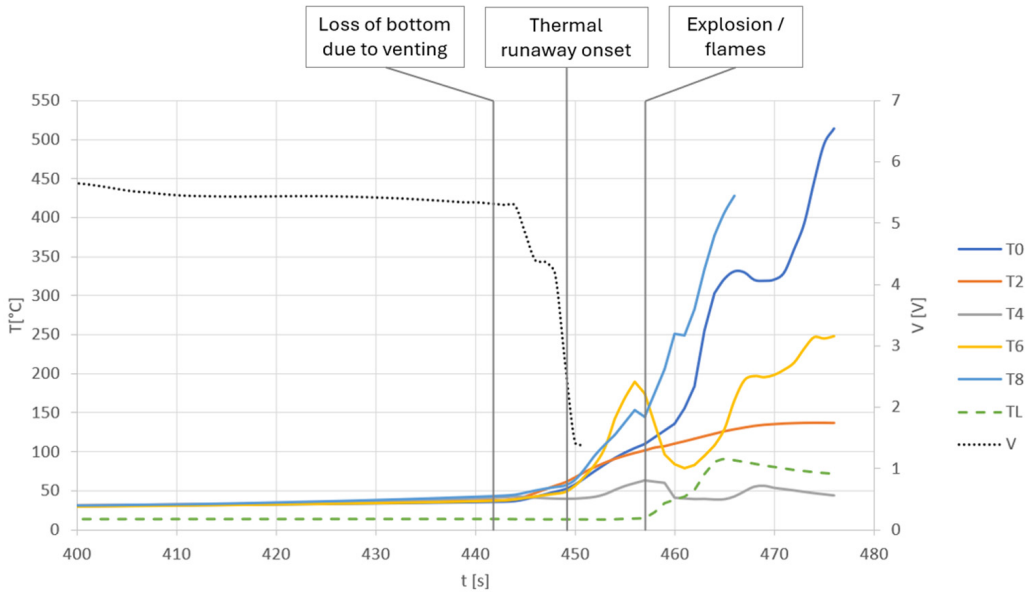

Figure 12. Temperature values of thermocouple T0–T8 on the surface of the cell; TL, temperature of the liquid and supply voltage for the test with synthetic ester.

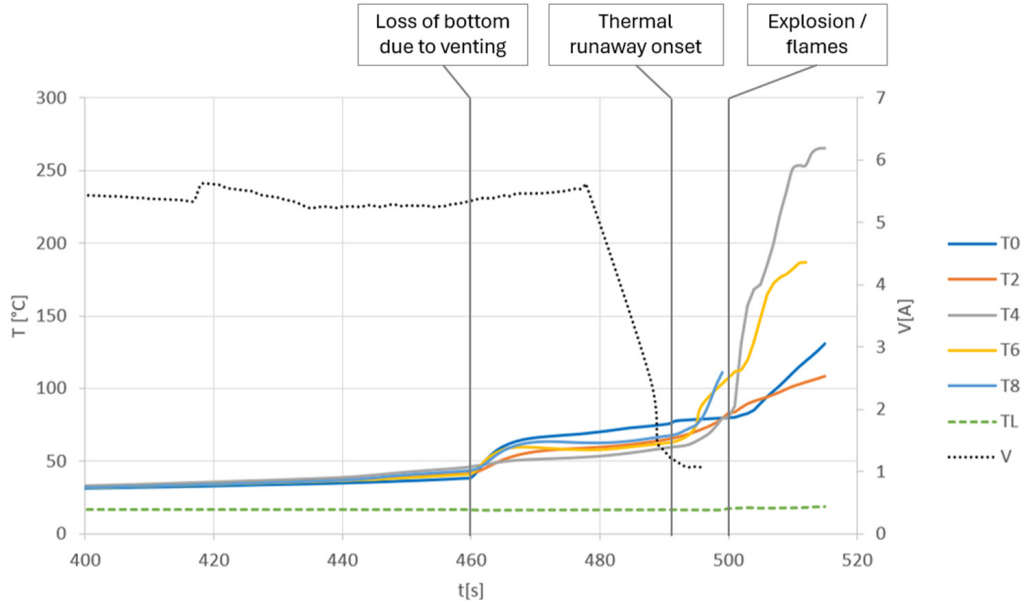

Figure 13. Temperature values of thermocouple T0-T8 on the surface of the cell; TL, temperature of the liquid and supply voltage for the test with silicone oil.

For a direct comparison, Figure 14 reports the temperature trends measured by the thermocouples that recorded the maximum temperature in each test. It is important to note that for the open-air test, the temperature curve presented in the graph is based on data collected by the thermal camera (see Figure 15) [7]); actually, in this case, the comparison between the measurements obtained by the thermocouples and those by the thermal camera indicated that the thermocouples detached from the cell surface well before the peak temperature of the thermal runaway was reached. To ensure clear visualization of the temperature trends, the curves in Figure 14 are plotted starting from 250 s up to their maximum values. The initial temperature offset observed in the open-air test is attributed to the higher ambient temperature at the time of the experiment (almost 23 °C, compared to the 11–17 °C range in the other tests).

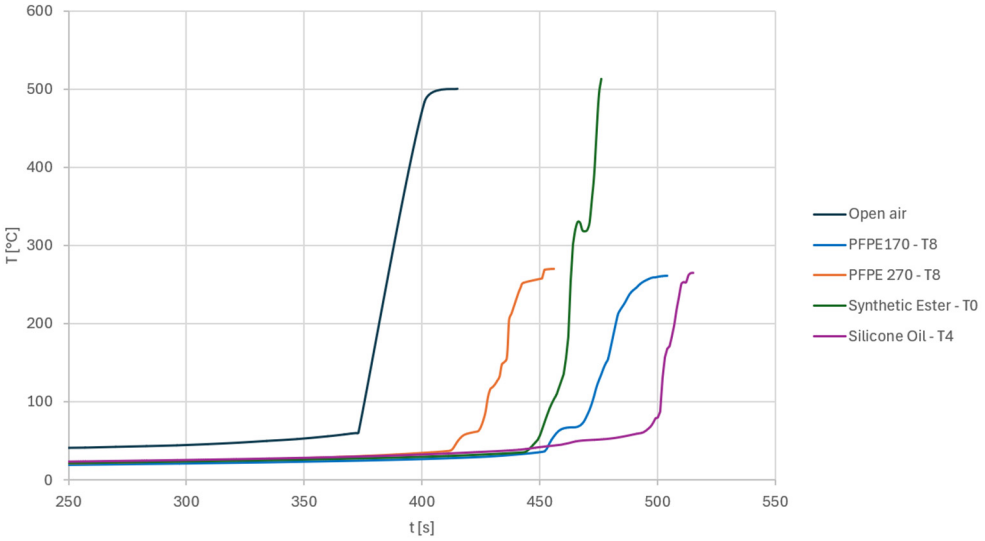

Figure 14. Temperature trends of thermocouples that recorded the maximum temperature in each test: for the open-air test, due to the early detachment of the thermocouples, the curve displayed refers to the thermo-camera readings.

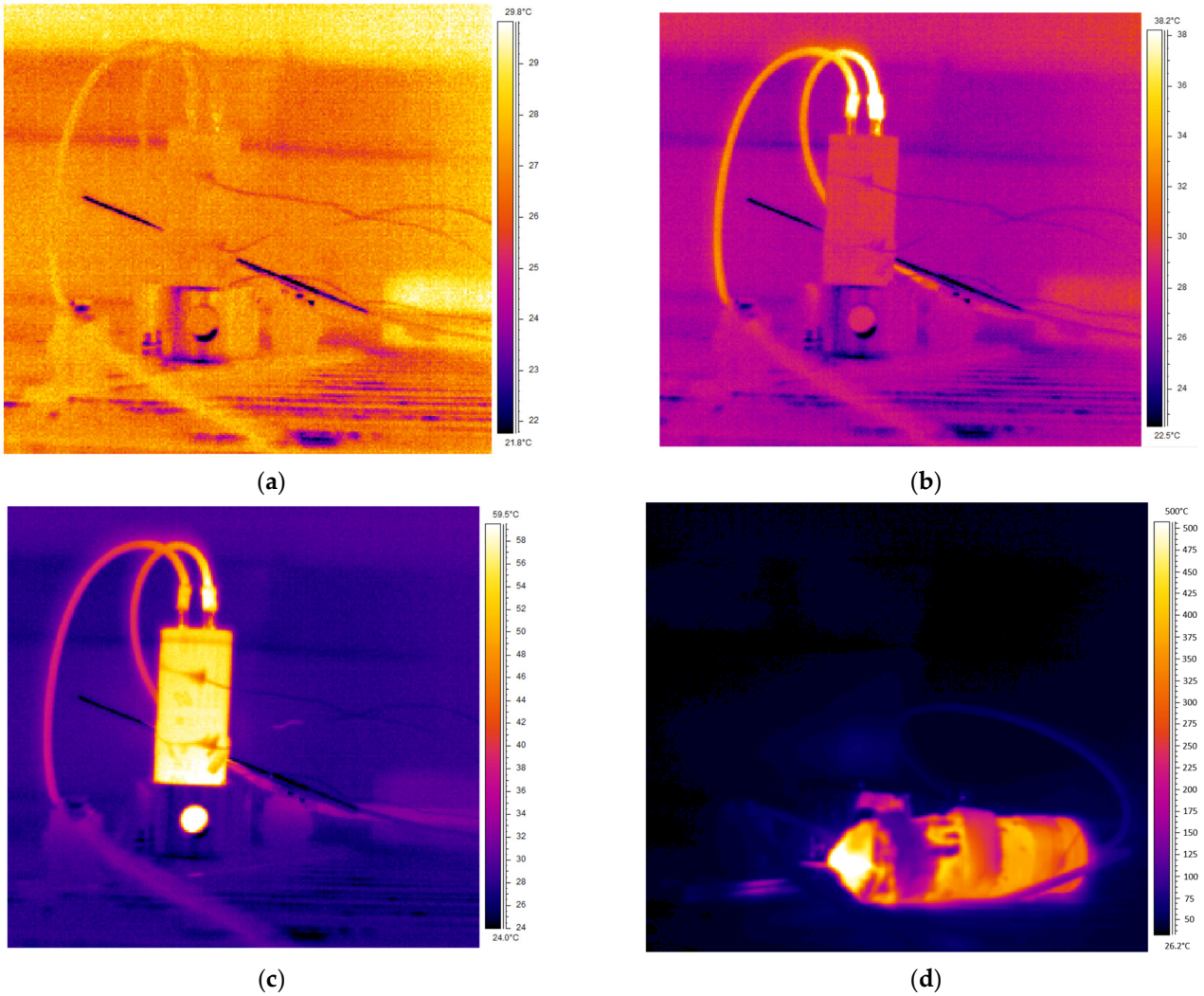

Figure 15. Thermal imaging camera frame of the explosion of LTO cell during the overcharge test in open-air conditions: (**a**) test start at 0 s, (**b**) at 62 s, (**c**) at 359 s, (**d**) and at 415 s, point of maximum temperature.

In the PFPE tests, the highest temperature corresponded with the maximum temperature of thermocouple T8. This result is consistent with the thermocouple's location which was positioned closest to the point where venting occurred. Conversely, in the tests involving synthetic ester and silicone oil, where T8 detached prematurely, the highest recorded temperatures were observed with T4 and T0, respectively. Except for in the synthetic ester test, thermocouple T4 recorded the lowest temperature values, likely due to its contact with the aluminum tray. The temperature of the surrounding liquid did not exhibit significant variations across the different tests. The beneficial effect of the presence of the dielectric fluids is apparent from Figure 14, with the efficiency increasing from the PFPE 270 to the silicone oil when a delay of more than 100 s was obtained.

Table 4 summarizes the maximum temperature recorded in each test, the maximum voltage during overcharging (before the first voltage drop), the average cell capacity measured with the battery cycler, and the State of Charge (SOC) achieved at the end of overcharging (the conclusion of the overcharge process was determined by identifying the last recorded voltage value before the final voltage drop occurred).

Table 4. Test characteristics for the cells.

Test	T Max [°C]	Max Voltage [V]	Average Cell Capacity @100% SOC [Ah]	SOC [%]	Liquid Fire
Open Air	500 (TC) [1]	5.29	8.87	146	-
PFPE170	261.6 (T8)	5.94	8.13	162	No
PFPE270	270.7 (T8)	5.88	8.13	156	No
Synthetic Ester	513.8 (T0)	5,84	8.13	159	Yes
Silicone Oil	265 (T4)	5,46	7.98	166	Yes

[1] Thermal imaging camera.

Even if in no case was the occurrence of thermal runaway totally prevented, the use of PFPE170 actually provided some benefits from a safety point of view. The tested fluorinated fluids, which have neither a flash point nor fire point, were effective in preventing the propagation of battery flames in the case of PFPE270, and even in suppressing battery flames in the case of PFPE 170. Besides this beneficial effect, the adoption of the dielectric fluids also introduced some significant safety concerns. In fact, with the exception of PFPE170, where only the venting of the cell was observed, in all other cases, a fire was generated after the thermal runaway. This was particularly intense in the case of synthetic ester and silicone oil, due to their involvement in the combustion process: the local temperatures exceeded their flash and fire points, and ignition was triggered by the short-circuiting of the cell. Further confirmation of the positive performance of PFPE170 is provided by UPLC-QToF-MS (Waters, Milford, MA, USA) analysis, where a comparison between the dielectric fluid before and after abuse testing showed no changes in the fluid's chemistry that could pose an additional risk.

3.2. Battery Pack Configuration Tests

A second set of tests was conducted to assess the effects of a single LTO cell under thermal runaway on adjacent cells within a battery pack (horizontal configuration, see Figure 3b) under overcharge abuse conditions.

Based on the results of the previous tests, PFPE170 was selected as the only fluid among those tested that effectively mitigates thermal runaway, preventing flame generation and propagation. Consequently, a benchmark test was performed under open-air conditions using a three-cell configuration, after which, a second test was carried out with the three cells immersed in PFPE170. Figures 16 and 17 display the most significant frames from the tests, captured by the fast camera. In these sets of figures, the first frame consistently depicts the initial conditions of the cell at the beginning of the test. The second frame shows the rupture of the cell bottom due to the internal accumulation of venting gasses. The third frame provides visualization of the venting phenomenon. The fourth frame shows the

instant of the explosion. The fifth frame depicts the moment after the explosion when the tray is clearly visible. The sixth frame reports the final condition at the end of the test.

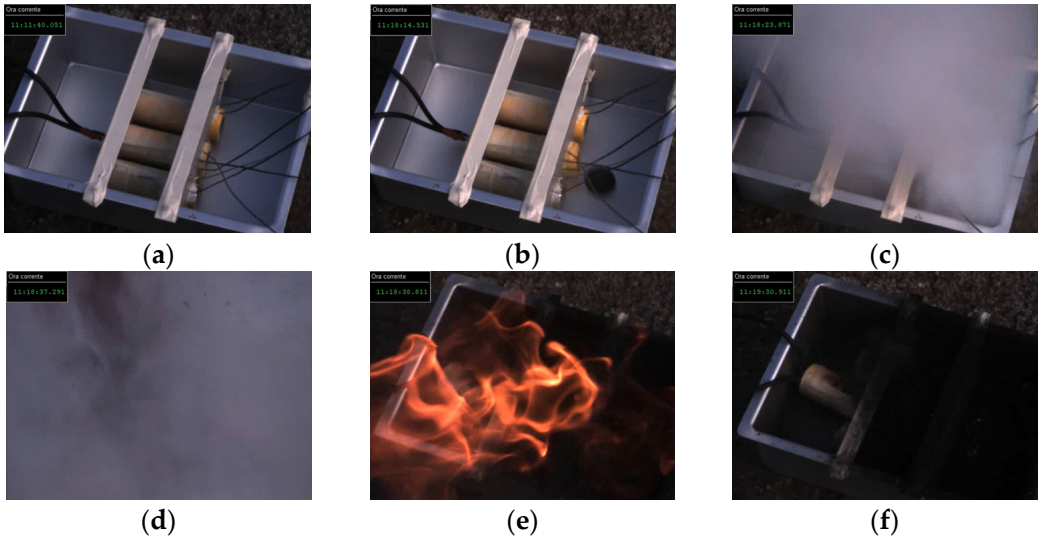

Figure 16. Battery pack in open-air conditions: (**a**) before venting; (**b**) loss of the bottom due to venting, (**c**) intensive venting, (**d**) explosion, (**e**) flame generation after the explosion, (**f**) after fire extinction.

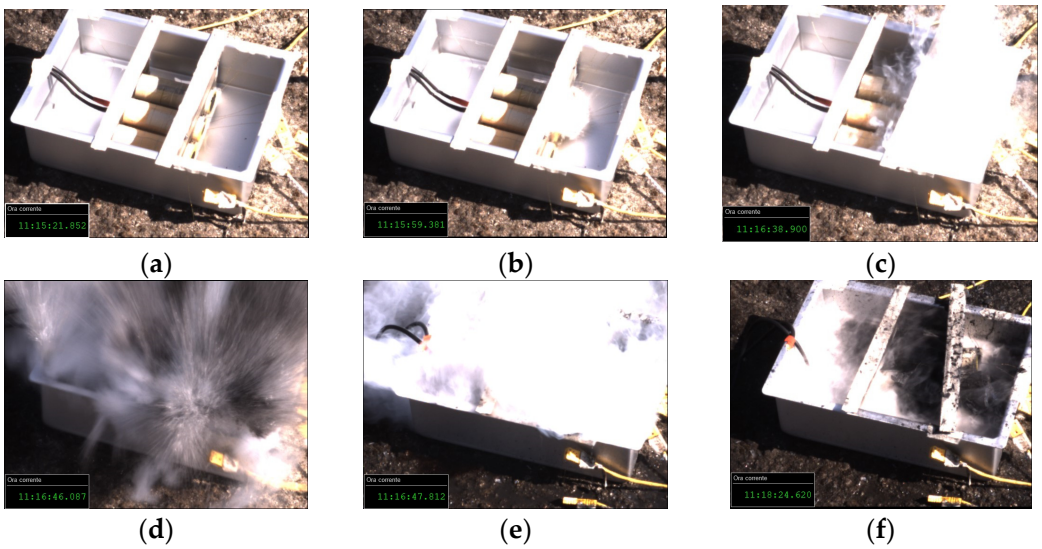

Figure 17. Battery pack immersed in PFPE170 sequence: (**a**) before venting, (**b**) loss of the bottom due to venting, (**c**) intensive venting, (**d**) explosion, (**e**) second venting after the explosion, (**f**) after intense venting.

Under open-air conditions, the overcharged cell experienced initial venting followed by a subsequent explosion, with significant flame generation. The adjacent cells did not experience any external visible damage. When PFPE170 was used as a thermal runaway mitigation strategy, the sequence of venting and explosion was similar to that observed in open-air conditions, but no flames were recorded. Additionally, a second intensive venting phase was observed after the explosion. Even in this case, the adjacent cells were not subjected to external damage.

Furthermore, the analysis of the previously defined characteristic time intervals, summarized in Table 5, indicates that the use of PFPE in a battery pack configuration appears to delay the achievement of maximum voltage.

Table 5. Timeline of the thermal runaway phases.

Test	t_{Vmax} [s]	t_r [s]	t_{TR} [s]	t_{ex} [s]	t_{Tmax} [s]
Open air	309	409	402	432	427
PFPE 170	367	452	475	498	501

To further investigate the test outcomes, a detailed analysis of temperature and voltage readings was conducted. The following sections provide a quantitative comparison of these parameters, offering insight into the thermal and electrical behavior of the cells under different test conditions. Figure 18 shows the thermographic images of the three-cell test layout, while Figures 19–22 illustrate the trends in supply voltage, ambient temperature, and cell surface temperature across the different tests, focusing on the temperature rise caused by the thermal runaway. Temperature readings from the thermocouples are reported starting from 370 s, as temperatures prior to this point are nearly uniform, allowing clearer visualization of the data. As for the previous tests, the temperatures are reported until the maximum value of the test or up to the detachment point of the thermocouple.

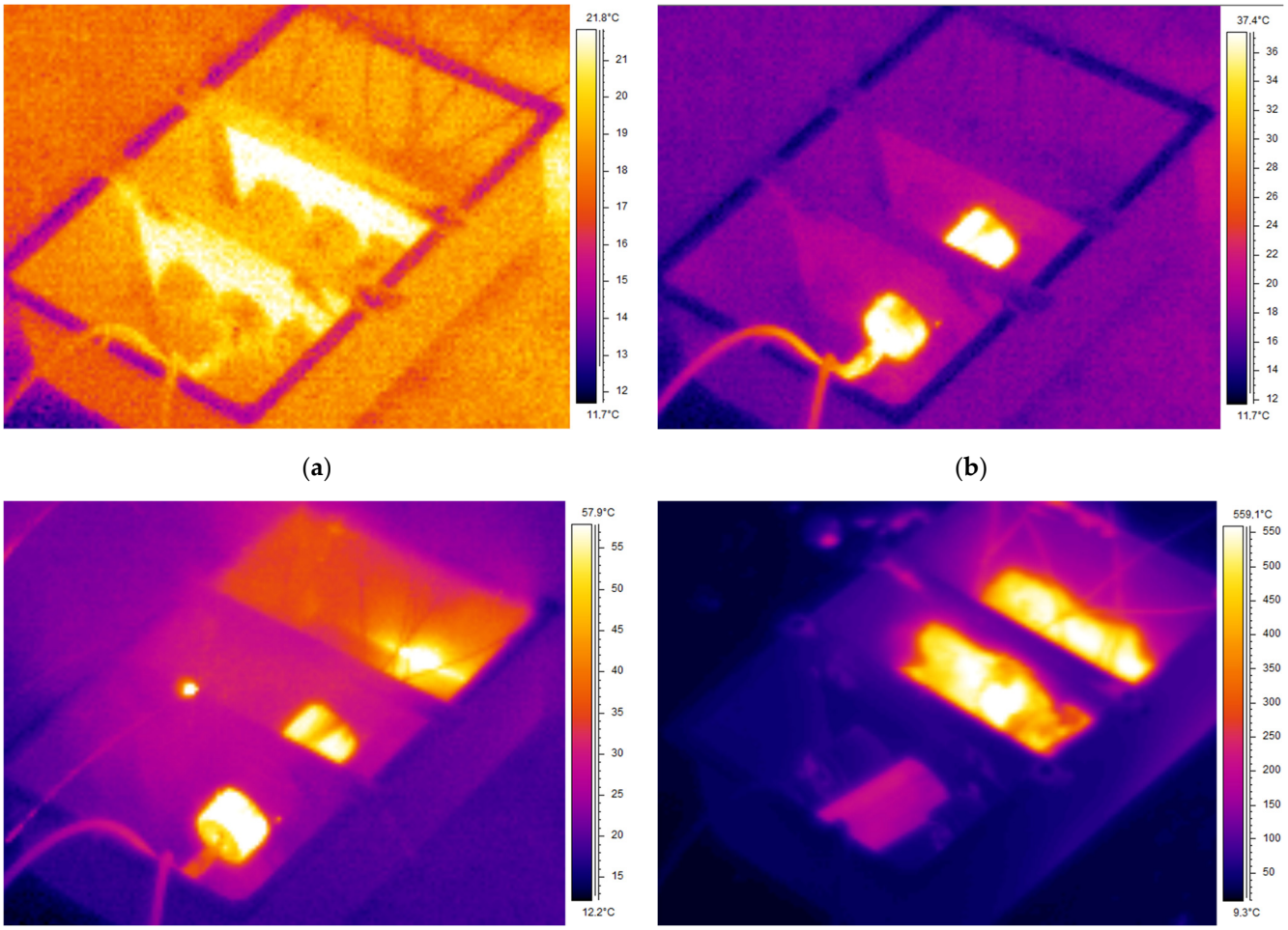

Figure 18. Thermographic images of the battery pack test layout in open-air conditions (**a**) test start, (**b**) t = 328 s, (**c**) t = 408s loss of the cell bottom and thermal runaway onset, (**d**) t = 429 s explosion.

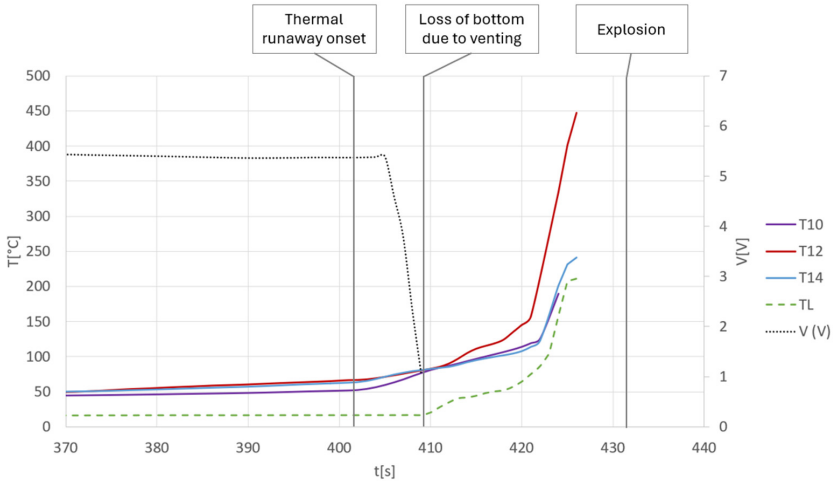

Figure 19. Temperature values of thermocouples on the surface of the abused cell; TL, ambient temperature and supply voltage for the test in battery pack configuration under open-air conditions.

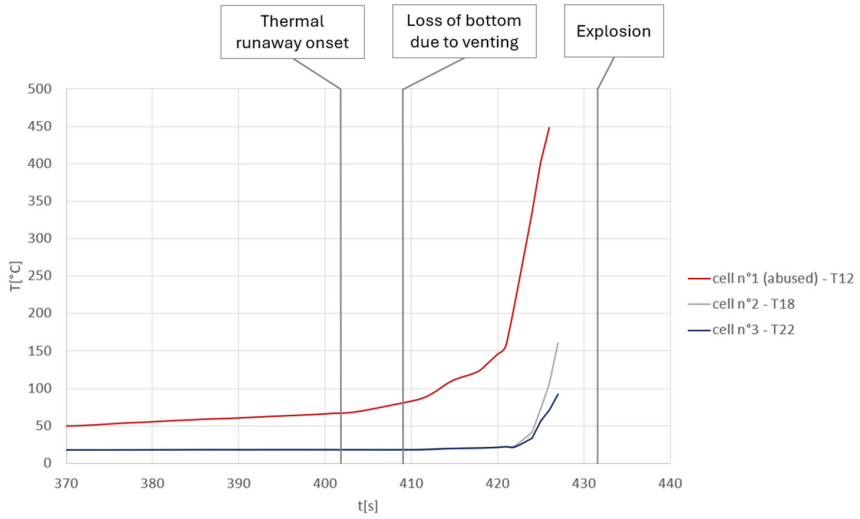

Figure 20. Comparison of the temperature trends of the thermocouple that recorded the maximum temperature of each cell in open air: T12 for the abused cell; T4 and T8 for the adjacent cells.

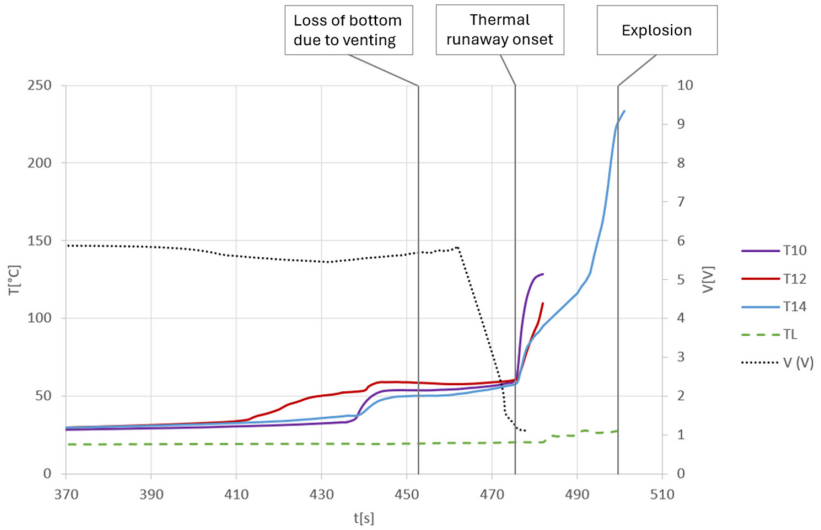

Figure 21. Temperature values of thermocouple on the surface of the abused cell; TL, temperature of the liquid and supply voltage for the test in battery pack configuration with the use of PFPE170.

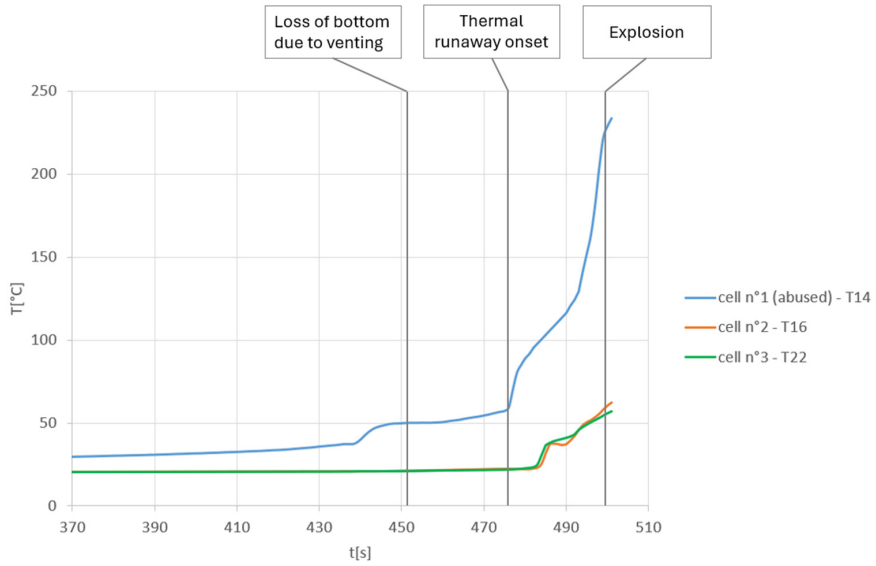

Figure 22. Comparison of the temperature trends of the thermocouple that recorded the maximum temperature of each cell with the use of PFPE170: T0 for the abused cell; T2 and T8 for the adjacent cells.

For comparison, Figure 23 presents a graphical analysis of temperature trends from thermocouple T14 in each test. Thermocouple T12, which reached the maximum temperature in the first test, was excluded from the comparison because it detached prematurely during the second test with PFPE170.

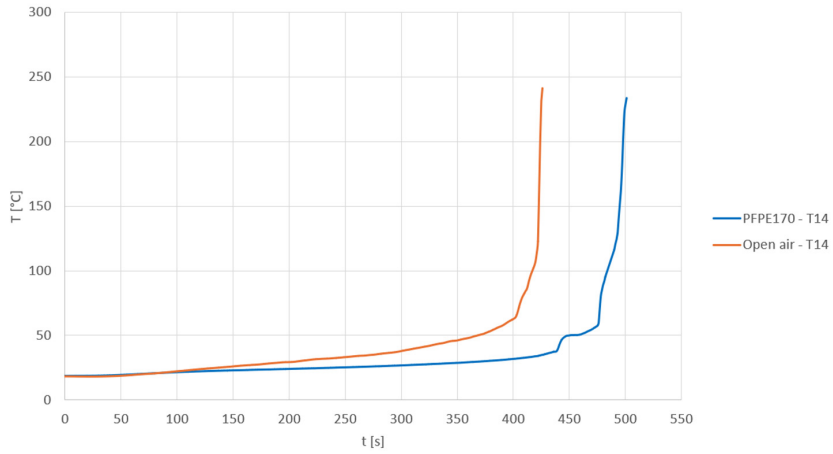

Figure 23. Temperature trends of thermocouple T14 in each test.

Under open-air conditions, the thermal runaway of the LTO cell followed a similar progression to that observed in the single-cell test, with the notable difference being the generation of more substantial flames. The maximum temperature recorded was 449.4 °C, as measured by thermocouple T12, which was positioned on the cell surface nearest to the venting point. This result is consistent with the expected temperature profile given the thermocouple location. However, the early detachment of some thermocouples limited the ability to fully capture all the phases of the thermal runaway in the temperature–time plot. Meanwhile, in the PFTE170 test, an explosion occurred without any flame generation. The maximum temperature recorded in the PFPE170 test matched the reading from thermocouple T14.

A significant comparison can be made regarding the surface temperatures of the cells adjacent to the abused cell in both tests. In the open-air test, the maximum temperatures recorded on the two adjacent cells were 160.7 °C (T4) and 92.3 °C (T8), respectively. In

contrast, during the second test with the cells immersed in PFPE170, the temperatures remained significantly lower and more uniform, being 62.5 °C (T2) and 57 °C (T8). This notable reduction highlights the effectiveness of PFPE170 in mitigating thermal propagation to neighboring cells during thermal runaway events.

Table 6 summarizes the maximum temperature reached in each test, the maximum voltage during overcharging (before the first voltage drop), the average cell capacity measured with the battery cycler, and the SOC achieved at the end of overcharging.

Table 6. Test characteristics for the three cells.

Test	T Max [°C]	Max Voltage [V]	Average Cell Capacity @100% SOC [Ah]	SOC [%]	Liquid Fire
Open air	449.4 (T12)	5.76	7.93	155	-
PFPE170	233.6 (T14)	5.87	8.22	162	No

4. Conclusions

The incidents related to the overcharging of lithium-ion batteries underscore the significant hazards posed by thermal runaway and highlight the need for effective containment strategies. While dielectric fluids have been widely studied for their applications in battery cooling and thermal management, the novelty of this work lies in investigating whether these fluids can also help to mitigate the thermal runaway in batteries. Specifically, this study investigated the potential of various dielectric fluids, evaluating whether these fluids can mitigate safety risks or, conversely, exacerbate them, by examining their impact on the consequences of thermal runaway in LTO cells.

Overcharge abuse tests were conducted on LTO cells immersed in four different fluids: two types of perfluorinated fluids with different boiling temperatures, synthetic ester, and silicone oil. The temperature at multiple points on the cell surface was monitored using thermocouples, while the qualitative behavior of the cell was assessed through thermal imaging and fast camera recordings. The results were compared with preliminary tests conducted in open-air conditions.

In the single-cell tests, the maximum temperatures varied across the different fluids, with synthetic ester exhibiting higher temperatures. Both silicone oil and synthetic ester demonstrated more pronounced explosive behaviors. All the tested liquid succeeded in delaying the onset of thermal runaway; however, PFPE170 emerged as the only and most effective, demonstrating the ability to prevent flame generation.

The performance of PFPE170 was further validated in a simplified battery pack scenario to assess the influence of thermal runaway in a single overcharged cell on adjacent cells both in open-air conditions and when immersed in PFPE170. Results from these tests confirmed that PFPE170 offers substantial mitigation benefits by retarding the thermal runaway and preventing fire generation.

In conclusion, the findings emphasize the importance of selecting appropriate dielectric fluids to enhance battery safety, particularly in high-risk scenarios. While dielectric fluids alone do not prevent the onset of thermal runaway, the performance of this particular perfluorinated fluid indicates its potential for enhancing battery safety, particularly in high-risk scenarios involving thermal runaway, offering a promising approach for managing its consequences. Future research should continue to explore and optimize dielectric fluid formulations and other containment strategies to address the challenges posed by thermal runaway in advanced battery technologies.

Author Contributions: Conceptualization, C.M. and A.N.M.; methodology, C.M., F.V. (Francesco Vitiello) and V.S.; formal analysis, C.M., A.N.M., F.V. (Francesco Vitiello) and L.C.; investigation, A.N.M., C.M., F.V. (Francesco Vitiello) and L.C.; data curation, A.N.M. and F.V. (Francesco Vitiello); writing—original draft preparation, A.N.M.; writing—review and editing, C.M., F.V. (Francesco Vitiello), L.C. and R.B.; visualization, A.N.M.; supervision, F.V. (Francesco Vellucci) and R.B.; project administration, C.M. All authors have read and agreed to the published version of the manuscript.

Funding: This research was funded by the Italian Ministry of Environment and Energy Security and ENEA.

Data Availability Statement: The original contributions presented in the study are included in the article, further inquiries can be directed to the corresponding author.

Conflicts of Interest: The authors declare no conflicts of interest.

References

1. European Commission, Clean Vehicles Directive. Available online: https://transport.ec.europa.eu/transport-themes/clean-transport/clean-and-energy-efficient-vehicles/clean-vehicles-directive_en (accessed on 5 November 2024).
2. Chen, W.; Liang, J.; Yang, Z.; Li, G. A Review of Lithium-Ion Battery for Electric Vehicle Applications and Beyond. *Energy Procedia* **2019**, *158*, 4363–4368. [CrossRef]
3. Dang, G.; Zhang, M.; Min, F.; Zhang, Y.; Zhang, B.; Zhang, Q.; Wang, J.; Zhou, Y.; Liu, W.; Xie, J.; et al. Lithium Titanate Battery System Enables Hybrid Electric Heavy-Duty Vehicles. *J. Energy Storage* **2023**, *74*, 109313. [CrossRef]
4. Nemeth, T.; Schröer, P.; Kuipers, M.; Sauer, D.U. Lithium Titanate Oxide Battery Cells for High-Power Automotive Applications—Electro-Thermal Properties, Aging Behavior and Cost Considerations. *J. Energy Storage* **2020**, *31*, 101656. [CrossRef]
5. Ding, Y.; Cano, Z.P.; Yu, A.; Lu, J.; Chen, Z. Automotive Li-Ion Batteries: Current Status and Future Perspectives. *Electrochem. Energ. Rev.* **2019**, *2*, 1–28. [CrossRef]
6. Belharouak, I.; Sun, Y.-K.; Lu, W.; Amine, K. On the Safety of the $Li_4Ti_5O_{12}$/$LiMn_2O_4$ Lithium-Ion Battery System. *J. Electrochem. Soc.* **2007**, *154*, A1083. [CrossRef]
7. Menale, C.; Constà, S.; D'annibale, F.; Scotini, A.; Sglavo, V. Experimental Investigation of the Overcharge Effects on Commercial Li-Ion Batteries with Two Different Anode Materials. *Chem. Eng. Trans.* **2021**, *86*, 457–462. [CrossRef]
8. Feng, X.; Ouyang, M.; Liu, X.; Lu, L.; Xia, Y.; He, X. Thermal Runaway Mechanism of Lithium Ion Battery for Electric Vehicles: A Review. *Energy Storage Mater.* **2018**, *10*, 246–267. [CrossRef]
9. Wen, J.; Yu, Y.; Chen, C. A Review on Lithium-Ion Batteries Safety Issues: Existing Problems and Possible Solutions. *Mater. Express* **2012**, *2*, 197–212. [CrossRef]
10. Wang, Q.; Ping, P.; Zhao, X.; Chu, G.; Sun, J.; Chen, C. Thermal Runaway Caused Fire and Explosion of Lithium Ion Battery. *J. Power Sources* **2012**, *208*, 210–224. [CrossRef]
11. Hendricks, C.; Williard, N.; Mathew, S.; Pecht, M. A Failure Modes, Mechanisms, and Effects Analysis (FMMEA) of Lithium-Ion Batteries. *J. Power Sources* **2015**, *297*, 113–120. [CrossRef]
12. Soares, F.J.; Carvalho, L.; Costa, I.C.; Iria, J.P.; Bodet, J.-M.; Jacinto, G.; Lecocq, A.; Roessner, J.; Caillard, B.; Salvi, O. The STABALID Project: Risk Analysis of Stationary Li-Ion Batteries for Power System Applications. *Reliab. Eng. Syst. Saf.* **2015**, *140*, 142–175. [CrossRef]
13. Ostanek, J.K.; Li, W.; Mukherjee, P.P.; Crompton, K.R.; Hacker, C. Simulating Onset and Evolution of Thermal Runaway in Li-Ion Cells Using a Coupled Thermal and Venting Model. *Appl. Energy* **2020**, *268*, 114972. [CrossRef]
14. Feng, X.; Ren, D.; He, X.; Ouyang, M. Mitigating Thermal Runaway of Lithium-Ion Batteries. *Joule* **2020**, *4*, 743–770. [CrossRef]
15. Shahid, S.; Agelin-Chaab, M. A Review of Thermal Runaway Prevention and Mitigation Strategies for Lithium-Ion Batteries. *Energy Convers. Manag. X* **2022**, *16*, 100310. [CrossRef]
16. Bubbico, R.; Greco, V.; Menale, C. Hazardous Scenarios Identification for Li-Ion Secondary Batteries. *Saf. Sci.* **2018**, *108*, 72–88. [CrossRef]
17. Suresh Patil, M.; Seo, J.-H.; Lee, M.-Y. A Novel Dielectric Fluid Immersion Cooling Technology for Li-Ion Battery Thermal Management. *Energy Convers. Manag.* **2021**, *229*, 113715. [CrossRef]
18. Liang, J.; Wang, F.; Feng, J.; Zhao, M.; Fang, R.; Pi, D.; Yin, G. A Hierarchical Control of Independently Driven Electric Vehicles Considering Handling Stability and Energy Conservation. *IEEE Trans. Intell. Veh.* **2024**, *9*, 738–751. [CrossRef]
19. Ortiz, A.; Delgado, F.; Ortiz, F.; Fernández, I.; Santisteban, A. The Aging Impact on the Cooling Capacity of a Natural Ester Used in Power Transformers. *Appl. Therm. Eng.* **2018**, *144*, 797–803. [CrossRef]
20. Roe, C.; Feng, X.; White, G.; Li, R.; Wang, H.; Rui, X.; Li, C.; Zhang, F.; Null, V.; Parkes, M.; et al. Immersion Cooling for Lithium-Ion Batteries—A Review. *J. Power Sources* **2022**, *525*, 231094. [CrossRef]
21. Sofia, U. Russo Paola Comparison Between 18650 Lithium-Ion Cells of Different Composition Subjected to Thermal Abuse. *Chem. Eng. Trans.* **2023**, *104*, 49–54. [CrossRef]
22. Ghiji, M.; Novozhilov, V.; Moinuddin, K.; Joseph, P.; Burch, I.; Suendermann, B.; Gamble, G. A Review of Lithium-Ion Battery Fire Suppression. *Energies* **2020**, *13*, 5117. [CrossRef]
23. Liu, Y.; Duan, Q.; Xu, J.; Chen, H.; Lu, W.; Wang, Q. Experimental Study on the Efficiency of Dodecafluoro-2-methylpentan-3-one on Suppressing Lithium-Ion Battery Fires. *RSC Adv.* **2018**, *8*, 42223–42232. [CrossRef] [PubMed]
24. Koster, D.; Marongiu, A.; Chahardahcherik, D.; Braun, C.F.; Schulte, D.; Figgemeier, E. Degradation Analysis of 18650 Cylindrical Cell Battery Pack with Immersion Liquid Cooling System. Part 1: Aging Assessment at Pack Level. *J. Energy Storage* **2023**, *62*, 106839. [CrossRef]

25. Andrenacci, N.; Menale, C.; Pasquali, M.; Felici, F.; Constà, S.; Sglavo, V. Studio per la Diagnostica Preventiva e la Gestione Della "Fuga Termica" per Sistemi di Accumulo Elettrochimico al Litio. *Report Ricerca di Sistema Elettrico 2023, (Accepted)*. Available online: https://www2.enea.it/it/ricerca-di-sistema-elettrico (accessed on 5 November 2024).
26. UNECE, Global Technical Regulation on the Electric Vehicle Safety (EVS), Addendum 20: Global Technical Regulation No. 20 ECE/TRANS/180/Add.20, 2018. Available online: https://unece.org/fileadmin/DAM/trans/main/wp29/wp29wgs/wp29gen/wp29registry/ECE-TRANS-180a20e.pdf (accessed on 5 November 2024).
27. Bruchhausen, M.; Hildebrand, S.; Kriston, A.; Ruiz, V.; Podias, A.; Pfrang, A. Evaluation of Detection Criteria for Thermal Runaway Experiments on Commercial Cells for Electric Vehicles. *Energy Rep.* **2023**, *10*, 510–519. [CrossRef]